A Simple Model of a Balanced Boundary Layer Coupled to a Large-Scale Convective Circulation

ROBERT J. BEARE

University of Exeter, Exeter, United Kingdom

MICHAEL J. P. CULLEN

Met Office, Exeter, United Kingdom

ABSTRACT

Many simple models of large-scale tropical circulations do not include a frictional boundary layer. A simple model is presented where the convective circulation is coupled to the boundary layer convergence. In the free troposphere, convection and boundary layer heating try to relax to a moist adiabat from the local sea surface temperature with a time scale τ_c, but other processes act to maintain a weak temperature gradient. There is a mass balance between radiatively driven subsidence and the large-scale convective mass flux. For a prescribed Gaussian surface temperature, the model predicts a mass flux that varies as $\tau_c^{-1/3}$ and a convective width proportional to its reciprocal. In the boundary layer, there can be significant horizontal temperature gradients and a balance between the pressure gradient and drag is assumed. Coupling between the two layers is mediated by the vertical velocity at the top of the boundary layer. The boundary layer constrains the circulation in three ways. First, it may lengthen the relaxation time scale compared to deep convection. Second, the evaporation in the nonconvecting region constrains the horizontal moisture advection. Third, it maintains a convective boundary layer where there is a convective mass flux; this condition cannot be satisfied if τ_c is too small or if the drag is too large, thus showing that such values are physically impossible. These results provide testable hypotheses concerning the physics and large-scale dynamics in weather and climate models.

1. Introduction

The response of large-scale convective circulations to the sea surface temperature (SST) is a key component of tropical dynamics. In weather and climate models, the interaction between the physical parameterizations and the large-scale dynamics is critical in the tropics. Improving such interactions presents an important frontier in future model development. Although the boundary layer mediates between the horizontally varying SST and the spatially uniform weak temperature gradient (WTG) layer, many simple models either neglect or partially represent it.

In the tropics, the boundary layer plays an important role in driving low-level convergence. Lindzen and Nigam (1987) consider the pressure gradient ''imprinted'' by the SST (herein referred to as the LN pressure gradient). The pressure gradient then induces convergence by Ekman balance. This effect, with certain modifications such as entrainment, has compared well against analyses in the studies of Back and Bretherton (2009) and Stevens et al. (2002). Back and Bretherton (2009) show analyses of boundary layer convergence and the convective precipitation; it is interesting that, although warm SST anomalies correspond to convergence, the horizontal scale of both the convergence and the precipitation is significantly narrower than the SST anomaly. Figure 1 illustrates the scenario of a broader SST anomaly than the regions of convergence and precipitation. A good test of a simple model is whether this narrowing can be reproduced.

Simple models are a useful tool for understanding tropical circulations and precipitation distributions. One example is Sobel and Neelin (2006), where they use a vertically truncated primitive-equation model to simulate the two effects of the convergence driven by thermodynamic instability and the LN pressure gradient. For a nonrotating case, they switch off the LN pressure

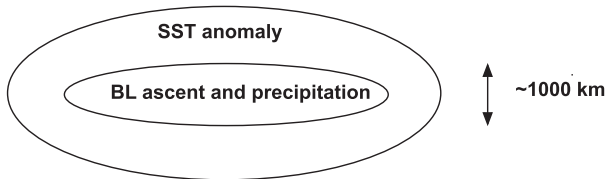*Corresponding author*: Robert J. Beare, r.j.beare@exeter.ac.uk

FIG. 1. A schematic illustrating the results of Back and Bretherton (2009), illustrating a broader SST anomaly than the regions of boundary layer ascent and precipitation.

gradient and conclude that it contributes to 25% of the precipitation. However, the tropospheric moist static energy dynamics (transport and flux divergence) were a more significant contributor to convergence. A simple model should thus include both thermodynamic and dynamic couplings with the boundary layer and surface.

Bretherton and Sobel (2002) describe a simple model of convectively driven Walker circulations. By combining mass and moist static energy balances with a strict quasi equilibrium for the convection, they simulate the sensitivity of the width of the convecting region to idealized cloud–radiative feedbacks. They note that their model could be extended to include a frictional boundary layer. Recently, Naumann et al. (2017) studied the impact of radiative cooling on a two-column mixed-layer model. They included the horizontal flow due to the LN pressure gradient between the columns, and showed a modification to the equilibrium state.

In this paper, we construct a minimal steady-state model of both the thermodynamic and dynamic feedbacks between the surface, boundary layer, and convection. Central to our model are the large-scale balances in the troposphere and the boundary layer. These are the WTG in the free troposphere and Ekman momentum balance associated with significant horizontal temperature gradients in the boundary layer (Beare and Cullen 2012). Within this framework, we will identify the factors that contribute to the narrowing of the convection region relative to the SST (Back and Bretherton 2009). Parameterization development often proceeds from process modeling at the small scale, then testing in a large-scale model. The disadvantage of that approach is the dynamical response is not fully considered in the development path of the parameterization. In contrast, here we start from the large scale and deduce the impact on simplified subgrid physics. The model will have a small number of controlling parameters such as the time scales associated with thermodynamic relaxation and boundary layer drag. The variation of the mass flux and precipitation with these parameters should reveal useful dependencies. These could provide testable hypotheses that can be applied in weather and climate models. For example,
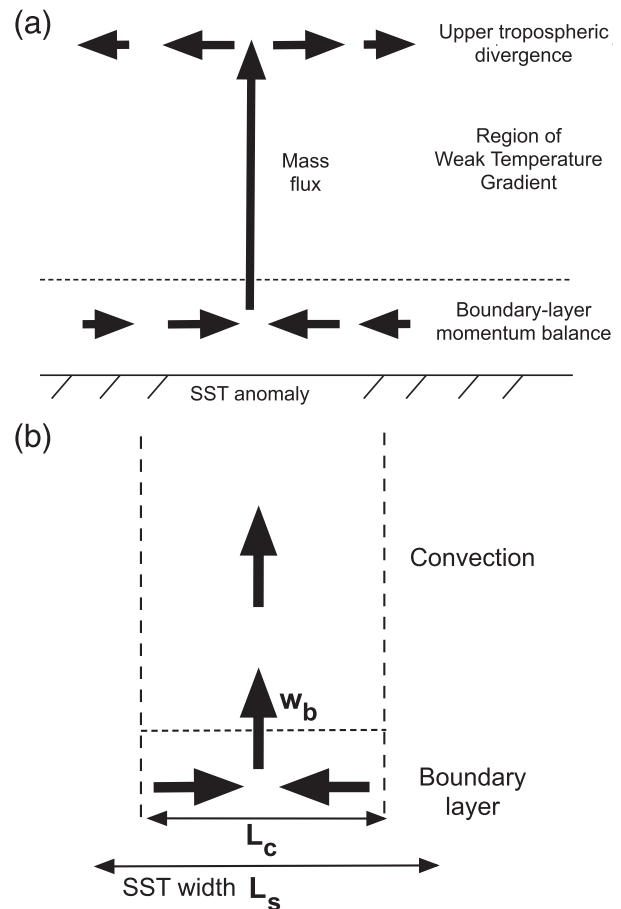

FIG. 2. Schematics of the flows and balances in the simple model: (a) horizontal flows in the boundary layer and upper troposphere; (b) coupling of the boundary layer convergence (where w_b is the boundary layer–top vertical velocity) to the convection flow.

if the relaxation rate of the convection scheme in a weather and climate model is altered, does the mass flux change in a similar way to that proposed by our simple model?

Section 2 describes the mathematical formulation of the simple model. We will then show example solutions in section 3.

2. Simple model

The model is illustrated in Fig. 2. It consists of a domain of width L_x and depth H. Within this domain is an idealized east–west Walker circulation that consists of boundary layer convergence, coupling to a vertical mass flux, and an upper-tropospheric divergence. The Coriolis force is neglected. Compared to other similar models (e.g., Bretherton and Sobel 2002), one novelty is the inclusion of a balanced boundary layer. The circulation is contained within a convecting region of width

L_c centered on $x = 0$, where x is the horizontal Cartesian coordinate. Critical to the model is the fact that L_c is allowed to vary with respect to the fixed width of the SST (L_s). The width of the boundary layer convergence is also L_c (Fig. 2b) so that the convective and boundary layer circulations are consistent. In addition to this momentum coupling, there is also coupling to the surface in terms of moisture and potential temperature relaxation.

There are two bulk layers in the vertical: the boundary layer and the WTG layer. This model, like others of its type, diagnoses the large-scale steady-state circulations associated with the boundary layer and convection (valid over the weekly to monthly time scale). It thus provides the basic state of the system and contrasts with other two-layer models (e.g., Wang and Rui 1990) that focus on the role of Kelvin–Rossby wave responses in the tropics.

The surface temperature T_s is prescribed as a Gaussian function in x with fixed width L_s and amplitude T_{s0}:

$$T_s = T_{s0} \exp\left(-\frac{x^2}{L_s^2}\right) + \theta_0, \qquad (1)$$

where θ_0 is a constant reference surface potential temperature. The side boundary conditions are fixed in terms of SST, momentum (zero inflow), and potential temperature profiles.

a. Convection proportional to deviation from WTG

In this section, we define the use of the WTG approximation in our model. In section 2d, we consider the additional roles of boundary layer stability and momentum balance. The atmospheric state above the boundary layer obeys the WTG approximation; it follows the moist adiabat determined by a particular surface temperature T_w and near-surface moisture mixing ratio q_w, illustrated by Fig. 3. This profile will be referred to as the WTG profile. Above the boundary layer, the WTG profile is distributed uniformly in the horizontal. At the edge of the convecting region, we assume convection turns off and so the WTG profile is the same as that determined by the SST and surface moisture mixing ratio q_s:

$$T_w = T_s(x = \pm L_c/2), \qquad q_w = q_s(x = \pm L_c/2). \qquad (2)$$

We assume convection results when the SST is greater than T_w. Figure 3 illustrates the assumed dynamic equilibrium that maintains the WTG profile. The convection and boundary layer attempts to warm and moisten the atmosphere beyond the WTG profile
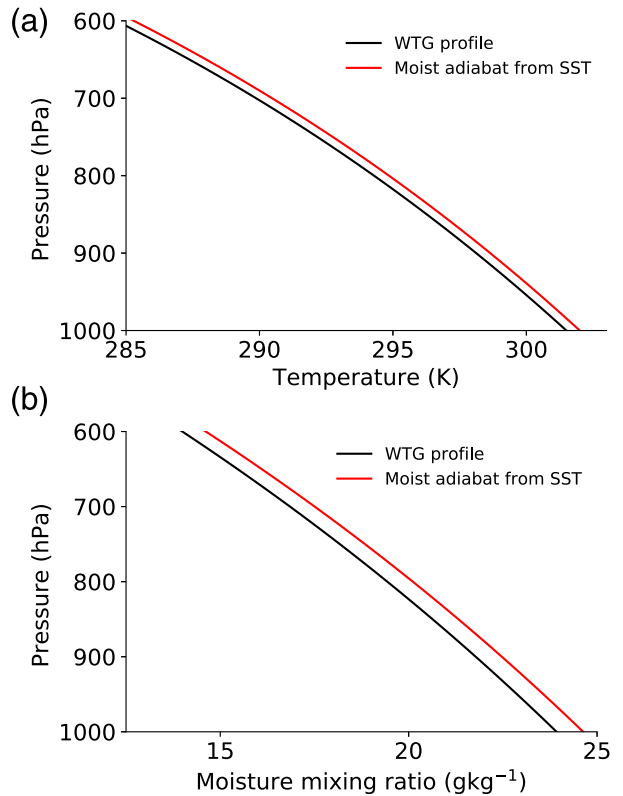

FIG. 3. Moist adiabat profiles for a surface temperature of $T_w = 301.5$ K, the WTG profile (black), and $T_s = 302$ K, the moist adiabat from SST (red). Shown are the (a) temperature and (b) moisture mixing ratio plotted against pressure, following Betts (1986). Surface values of the WTG and SST moisture profiles in (b) are given by q_w and q_s, respectively.

toward the moist adiabat defined by the SST. Gravity waves (Raymond and Zeng 2005), cloud–radiative feedbacks, and other transients are assumed to act in the opposite sense and exactly balance the thermodynamic tendencies from boundary layer and convection. Thus the WTG profile remains undisturbed above the boundary layer. Consistent with this scenario, the convective mass flux and precipitation are parameterized as deviations from the WTG profile:

$$M_c = \gamma_c \frac{T_s - T_w}{\tau_c}, \qquad |x| \le L_c/2, \qquad (3)$$

$$\frac{P}{L\rho_0 H} = \gamma_q \frac{q_s - q_w}{\tau_c}, \qquad |x| \le L_c/2, \qquad (4)$$

where M_c is the mass flux divided by density (herein referred to simply as mass flux), P the precipitation flux (W m^{-2}), L the latent heat of vaporization, and ρ_0 is the surface density. The constants of proportionality (γ_c and γ_q) scale the respective potential temperature and

moisture deviations from WTG to give physically realistic values of M_c and P. They account for any changes in units and also for vertical variations in the reference profiles (Fig. 3). We have also combined the large-scale ascent and moist convective mass flux (subgrid and resolved) into M_c.

The sensible heat flux divergence across the boundary layer $\mathscr{F}_b$ combines with the heating rate due to moist convection $\mathscr{H}_c$:

$$\frac{T_s - T_w}{\tau_c} \propto \mathscr{H}_c + \frac{\mathscr{F}_b}{h}, \tag{5}$$

where h is the boundary layer depth. This combination of convection and boundary layer thermodynamics is represented by a finite relaxation time scale, analogous to Betts (1986). We envisage the time scales from convection τ_{cc} and the boundary layer τ_{cb} are combined as

$$\frac{1}{\tau_c} = \frac{A_c}{\tau_{cc}} + \frac{A_b}{\tau_{cb}}. \tag{6}$$

We refer to τ_c as the relaxation time scale throughout. In the case where the convective relaxation dominates ($A_c \gg A_b$), the same time scale as Betts (1986) of 2 h is used. A larger value of τ_c (here we will use 10 h) is used when there is a greater weighting toward the slower boundary layer thermodynamic adjustment. We thus consider values of τ_c up to 10 h.

In the limit of zero τ_c, this formulation reverts to strict quasi equilibrium; the WTG profile collapses to a moist adiabat starting from the maximum SST. This can be seen mathematically in Eq. (3) where, assuming $T_s - T_w \sim \tau_c^\alpha$, for $\alpha < 1$, then as $\tau_c \to 0$, $M_c \to \infty$ and $T_w \to T_s \to \max(T_s)$. This property is a benefit of using a single relaxation time scale, as the limit of the maximum SST is clearly followed. We note that, in this limit, others used the gross moist stability to parameterize the vertical velocity (e.g., Bretherton and Sobel 2002). In these instances, the vertical velocity is dependent on the differences between evaporation and radiation flux divergences across the troposphere. We have chosen instead to focus our study on the roles of boundary layer balance and convective efficiency. Thus we have adopted a type of the *relaxed* quasi-equilibrium approach of Raymond and Zeng (2005), with a dynamic equilibrium between convective heating and gravity wave cooling.

b. Mass balance in WTG layer

As a background state in the WTG layer, we assume a thermodynamic balance between constant radiative cooling and adiabatic warming. In the WTG layer, a constant subsidence velocity w_s results:

$$w_s = -\frac{R}{\rho S c_p H}, \tag{7}$$

where R is a positive constant radiative flux change across the troposphere, S is a mean vertical potential temperature gradient, and c_p is the specific heat capacity of air at constant pressure. We assume a constant mean tropospheric density ρ that accounts in a simple way for the vertical variation of density relative to its surface value. The subsidence is uniform across the troposphere. This is in contrast to the typical assumptions in mass flux parameterization where it is confined to the grid box in question (Kuell et al. 2007). In a simple model such as ours, we have the freedom to distribute w_s in a more physically realistic way. We can also explore the consequences of the width of convection without the constraint of a model grid box.

The combination of the WTG approximation and hydrostatic balances means that horizontal pressure gradients are negligible above the boundary layer. As a consequence, the horizontal momentum equation is not required and only the mass balance remains for the dynamics. In the absence of horizontal flow at the side boundaries, mass conservation means the convective mass flux balances the subsidence:

$$L_x w_s + L_c \langle M_c \rangle = 0. \tag{8}$$

The angle brackets indicate the horizontal average over the convection region.

c. Maximum mass flux as a function of τ_c

Combining Eqs. (1)–(3) gives an equation for the maximum mass flux:

$$M_{c0} = \frac{\gamma_c T_{s0}}{\tau_c} \left[1 - \exp\left(-\frac{L_c^2}{4L_s^2}\right) \right], \tag{9}$$

where the maximum value is indicated by an additional "0" subscript. If we Taylor expand this expression for sufficiently small values of L_c/L_s we have

$$M_{c0} \simeq \frac{\gamma_c T_{s0}}{\tau_c} \frac{L_c^2}{4L_s^2}. \tag{10}$$

The maximum mass flux is proportional to its mean over the convecting region, allowing us to write Eq. (8) as $M_{c0} \propto -w_s L_x / L_c$, substituting into Eq. (10) to give

$$M_{c0}^3 \propto \left(\frac{-w_s L_x}{L_s}\right)^2 \frac{\gamma_c T_{s0}}{\tau_c} \tag{11}$$

$$\Rightarrow M_{c0} \propto \left(\frac{-w_s L_x}{L_s}\right)^{2/3} \left(\frac{\gamma_c T_{s0}}{\tau_c}\right)^{1/3}, \tag{12}$$

$$L_c \propto \left(\frac{-w_s L_x L_s^2 \tau_c}{\gamma_c T_{s0}} \right)^{1/3}. \qquad (13)$$

Equations (12) and (13) indicate $\tau_c^{-1/3}$ and $\tau_c^{1/3}$ power laws for the maximum mass flux and convective width, respectively. The equations also show interesting dependencies on subsidence and the SST (maximum and width). For example, increasing the maximum SST leads to an increase in the mass flux and a decrease in the convective width with a one-third power law.

The effect of the mass balance on the horizontal scale and magnitude of mass flux is present in other simple models such as Bretherton and Sobel (2002). However, the differences lie in the way mass flux is closed. In Bretherton and Sobel (2002) the mass flux (equivalent to the large-scale vertical velocity in their model) is closed using a gross moist stability assuming strict quasi equilibrium. Here, we assume a dynamical equilibrium between convection and other transients. Such an assumption makes the role of convective efficiency central to the model and something that can be diagnosed from weather and climate models.

d. Coupling to boundary layer

Given the previous definition of the mass flux in the WTG layer, we now determine the boundary layer potential temperature and winds that are consistent with it using momentum balance. The boundary layer is assumed to be well mixed above the surface, with potential temperature θ_b. While the SST is fixed, θ_b is allowed to vary in x. Figure 4 shows typical vertical profiles for a convective boundary layer (CBL; $T_w < \theta_b < T_s$) and stable boundary layer (SBL; $T_w > \theta_b > T_s$). For the boundary layer to be physically realistic, it needs to be in the CBL state in the convection region. We will return to this point later in section 3c.

All variables apart from the boundary layer top vertical velocity w_b are vertical averages over the boundary layer. In contrast to the WTG layer, the boundary layer has significant horizontal gradients of potential temperature. Vertically integrating the Boussinesq hydrostatic balance across the boundary layer gives the geopotential perturbation ϕ_b:

$$\phi_b = -\frac{h}{2} \frac{g(\theta_b - \theta_0)}{\theta_0}, \qquad (14)$$

where h and g are the boundary layer depth and gravitational acceleration, respectively. We assume the geopotential perturbation is zero at $z = h$, and the
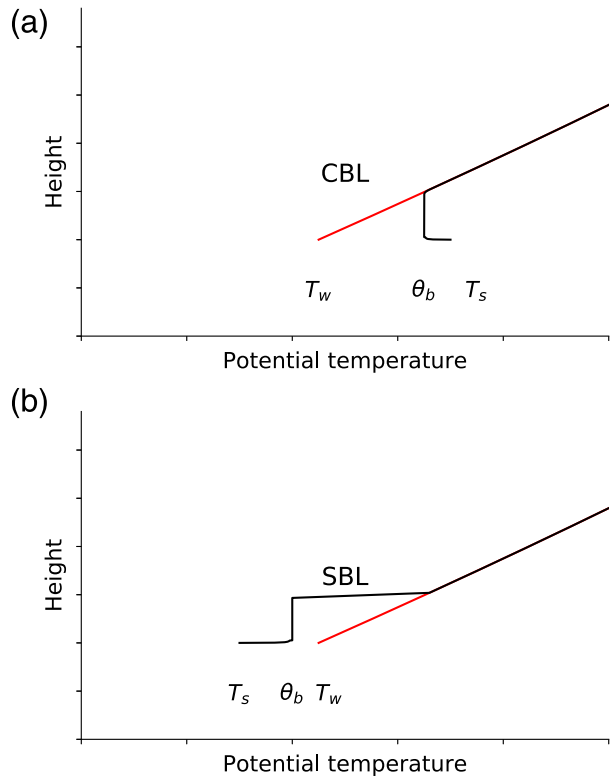

FIG. 4. Schematics of vertical profiles of potential temperature for the boundary layer (black) with respect to the WTG profile (red) for the (a) CBL ($T_w < \theta_b < T_s$) and (b) SBL ($T_w > \theta_b > T_s$).

factor of $h/2$ appears as the mean value of the geopotential corresponds to the value in the middle of the boundary layer. An Ekman momentum balance is assumed:

$$-\frac{u_b}{\tau_b} = \frac{d\phi_b}{dx}. \qquad (15)$$

Since the Coriolis parameter is zero, Eq. (15) is simply a balance between geopotential gradient and drag terms, sometimes also referred to as Darcy's balance (Beare and Cullen 2012). The time scale τ_b is a Rayleigh boundary layer time scale and is associated with a bulk momentum diffusion K_b such that $\tau_b \sim h^2/K_b$. The balance applies strictly for advective time scales very much greater than τ_b (of order 1 week). Assuming constant density, mass balance gives the boundary layer top vertical velocity

$$w_b = -\frac{du_b}{dx} h. \qquad (16)$$

Combining Eqs. (14)–(16) gives an expression for u_b and w_b in terms of the first and second derivatives of the mixed-layer potential temperature, respectively:

$$u_b = \frac{\tau_b g h}{2\theta_0} \frac{d\theta_b}{dx}, \qquad (17)$$

$$w_b = -\frac{\tau_b g h^2}{2\theta_0} \frac{d^2\theta_b}{dx^2}. \qquad (18)$$

The imposition of balance means that both the horizontal and vertical velocity are "slaved" to the mixed-layer potential temperature, or vice versa [Eqs. (17) and (18)]. We assume continuity of the vertical velocity at the boundary layer top with the sum of convective mass flux and subsidence. This is similar to Lindzen and Nigam (1987), who assume the mass flux scales with the boundary layer convergence. Equation (18) can now be stated in reverse, such that the curvature of the boundary layer potential temperature is now set in proportion to ascent in the convection region:

$$-\frac{\tau_b g h^2}{2\theta_0} \frac{d^2\theta_b}{dx^2} = w_b = M_c + w_s. \qquad (19)$$

Equation (19) provides an explanation of why horizontal temperature gradients can exist within the boundary layer, while they do not in the WTG layer above. Our model is based around the WTG temperature profile and the boundary layer is calculated to be consistent with it. This contrasts with the view that the boundary layer potential temperature is fixed, determining the vertical velocity and thus the mass flux (Lindzen and Nigam 1987).

We also assume that the boundary layer is neutrally stratified at the edge of the convecting region:

$$\theta_b = T_w, \qquad x = \pm L_c/2. \qquad (20)$$

Equations (19) and (20) are solved for θ_b using finite differences and a tridiagonal matrix solver with a horizontal grid length of 5 km (Press et al. 2007).

e. Tropospheric horizontal winds

We can now proceed to diagnose the horizontal winds above the boundary layer using mass balance. For each column, we assume the vertical profile given by Fig. 5. Since it is a mixed layer with uniform convergence with height, the vertical velocity increases linearly over the boundary layer depth until it reaches its maximum value. To match the vertical velocity at the boundary layer top, the sum of mass flux and subsidence is assumed uniform with height until near the tropopause. Over a distance d below the tropopause, the mass flux decreases linearly to zero. The subsidence decreases to zero over the same depth in order to satisfy a rigid lid condition. The upper-tropospheric wind u_u is thus determined from continuity by
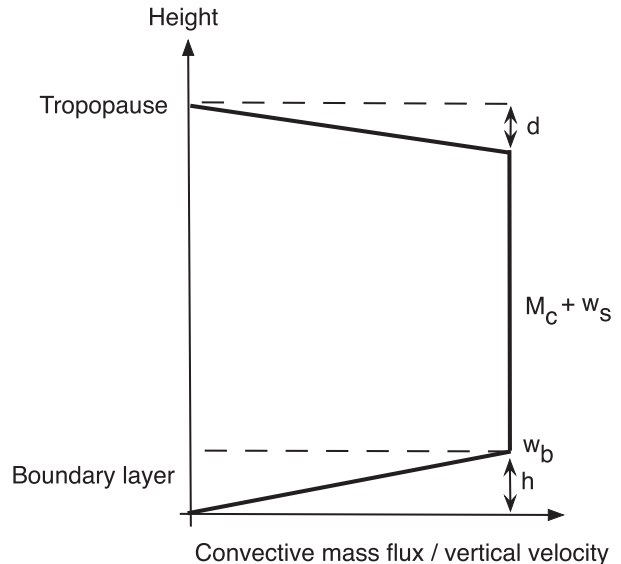

FIG. 5. Vertical profile of the mass flux, subsidence, and boundary layer vertical velocity for each vertical column. Since it is a mixed layer, the vertical velocity increases linearly over the depth h until it reaches its maximum value w_b. The sum of mass flux and subsidence $(M_c + w_s)$ is continuous with w_b (to avoid spurious convergence/divergence). Then $M_c + w_s$ decreases linearly over a depth d below the tropopause. In nonconvective regions $M_c = 0$.

$$\frac{du_u}{dx} = \begin{cases} \dfrac{M_c + w_s}{d} & |x| \le L_c/2, \\[2mm] \dfrac{w_s}{d} & \text{otherwise.} \end{cases} \qquad (21)$$

f. Moisture budget

Above the boundary layer, within the convection region, we assume the moisture profile is saturated. Since the reference WTG temperature profile is horizontally uniform within the convection region, saturation means that the moisture mixing ratio is also horizontally uniform. Outside the convection region, the advective fluxes of moisture maintain a steady-state moisture distribution. Values of boundary layer and upper-tropospheric horizontal winds (u_b, u_u) at the left edge of the convection region $(x = -L_c/2)$ are given by u_{bc} and u_{uc}, respectively. Values of moisture at the edge of the convection region in the boundary layer and upper troposphere are given by q_{bc} and q_{uc}, respectively, where

$$q_{bc} = q_{wz}(h), \qquad (22)$$

$$q_{uc} = q_{wz}(H), \qquad (23)$$

and q_{wz} is the WTG moisture profile as a function of height. We have also assumed that the lifting condensation
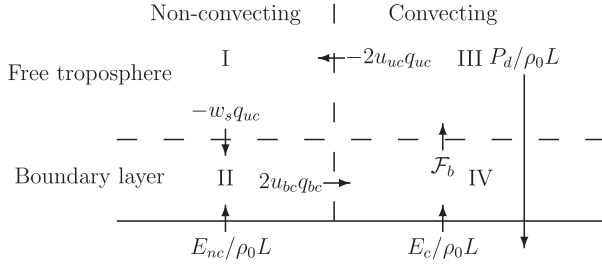
FIG. 6. The moisture fluxes assumed between (right) convecting and (left) nonconvecting boundary layer and free-troposphere regions. All fluxes shown are positive. Boxes are labeled I, II, III, and IV for ease of reference in the text.

TABLE 1. Constants and parameters used in control simulation.

Symbol	Value	Symbol	Value
L_s	1060.7 km	T_{s0}	2 K
L_x	2500 km	H	10 km
R	$100 \, \text{W m}^{-2}$	S	$5 \, \text{K km}^{-1}$
ρ	$0.77 \, \text{kg m}^{-3}$	w_s	$-2.6 \, \text{mm s}^{-1}$
τ_c	2 h	τ_b	12.5 h
h	2.5 km	d	1.5 km
γ_c	$500 \, \text{m K}^{-1}$	γ_c	0.15
ρ_0	$1.275 \, \text{kg m}^{-3}$	θ_0	300 K

level is at the top of the boundary layer, which is also well mixed in moisture mixing ratio. Figure 6 shows the moisture fluxes assumed for four boxes (labeled I, II, III, and IV). We evaluate the domain-averaged budgets for these boxes as

$$\text{Box I:} \quad -\frac{w_s q_{uc}}{H-h} = -\frac{2u_{uc}q_{uc}}{L_x}, \quad (24)$$

$$\text{Box II:} \quad \frac{E_{\text{nc}}}{\rho_0 L h} = \frac{2u_{bc}q_{bc}}{L_x} + \frac{w_s q_{uc}}{h}, \quad (25)$$

$$\text{Box III:} \quad \frac{\mathscr{F}_b}{H-h} = -\frac{2u_{uc}q_{uc}}{L_x} + \frac{P_d}{\rho_0 L(H-h)}, \quad (26)$$

$$\text{Box IV:} \quad \frac{E_c}{\rho_0 L h} = \frac{\mathscr{F}_b}{h} - \frac{2u_{bc}q_{bc}}{L_x}, \quad (27)$$

where $\mathscr{F}_b$ is the domain-averaged vertical moisture flux at the top of the boundary layer and P_d is the domain-averaged precipitation. The quantities E_{nc} and E_c are the domain-averaged evaporative fluxes for the non-convecting and convecting regions, respectively. For example, the domain averaging of horizontal moisture advection leads to terms such as $2u_{bc}q_{bc}/L_x$ for regions II and IV. Eliminating the subsidence term from Eqs. (24) and (25) and $\mathscr{F}_b$ from Eqs. (26) and (27) gives

$$\frac{E_{\text{nc}}}{\rho_0 L h} = \frac{2u_{bc}q_{bc}}{L_x} + \frac{H-h}{h}\frac{2u_{uc}q_{uc}}{L_x}, \quad (28)$$

$$E_c + E_{\text{nc}} = P_d. \quad (29)$$

Equation (29) shows that evaporation balances precipitation when averaged over the whole domain. Equation (28) shows that E_{nc} balances horizontal moisture advection; physically appropriate values of E_{nc} may act as a constraint on horizontal moisture advection and thus on the whole model.

Table 1 gives the constants and parameters used in the control configuration of our simple model. The choice of $T_{s0} = 2 \, \text{K}$ follows from the east–west variation in SST used in the GCM simulations of Seager et al. (2003). We will then vary τ_c, τ_b, w_s, and T_{s0} in order to understand the roles of convection efficiency, boundary layer balance, radiative forcing, and SST in controlling the width L_c and magnitude M_c of the mass flux.

3. Results

We start by showing the results of combining mass balance and the relaxation parameterization in the WTG layer. We then include results of coupling to a boundary layer momentum balance.

a. Mass flux in WTG layer

The positioning of the WTG temperature T_w relative to the SST is shown in Fig. 7. For a given set of parameters, the WTG temperature is, by definition, uniform in x. While the SST remains fixed, the WTG temperature increases toward the maximum SST as τ_c decreases. The convection width exists between the two intersections of the WTG line and the SST, so thus
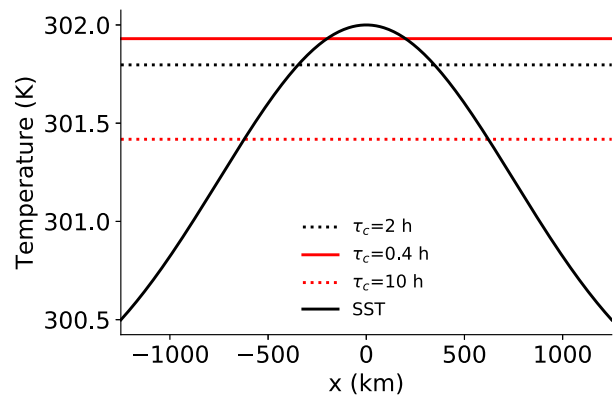

FIG. 7. The SST (black) and WTG temperatures for the control ($\tau_c = 2$ h; black dotted), $\tau_c = 0.4$ h (red), and $\tau_c = 10$ h (red dotted).
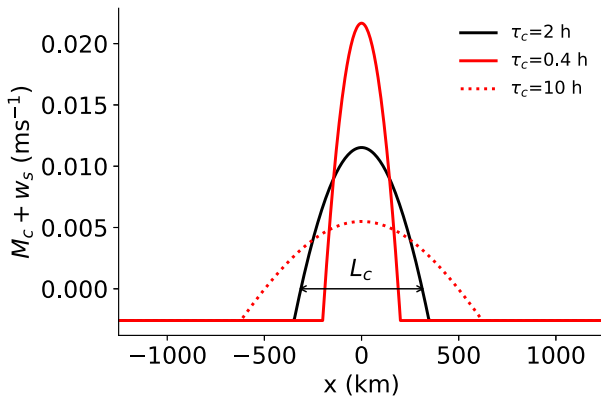
FIG. 8. The sum of subsidence and mass flux for the WTG layer (the same as the vertical velocity at the boundary layer top). Shown are profiles for the control ($\tau_c = 2$ h; black), $\tau_c = 0.4$ h (red), and $\tau_c = 10$ h (red dotted). The convective width for $\tau_c = 2$ h is marked by the horizontal arrow.
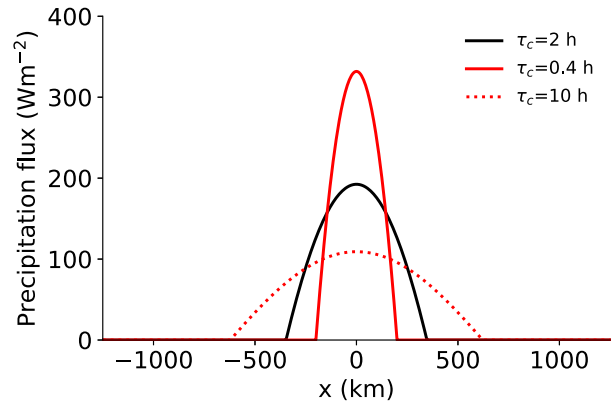

FIG. 9. The precipitation flux for the control case ($\tau_c = 2$ h; black), $\tau_c = 0.4$ h (red), and $\tau_c = 10$ h (red dotted). The precipitation flux is equal to the evaporation flux.

also decreases. In contrast, when τ_c increases to 10 h, the WTG temperature decreases. Consistent with this picture, Fig. 8 shows the horizontal distribution of the sum of subsidence and mass flux for three different values of τ_c. The largest value of $\tau_c = 10$ h accounts for the lengthening of time scale by the boundary layer from the 2 h used by Betts (1986); it also reflects the lack of north–south effects. Within the convection region, the positive mass flux dominates; outside the convection region is the uniform subsidence. Mass balance [Eq. (8)] means that the horizontal mean is maintained at zero. The uniform subsidence is critical in allowing the width and amplitude of the mass flux to adjust with convection efficiency. As τ_c decreases from 2 to 0.4 h, the maximum mass flux increases [Eq. (3)] and the width of the convection region has to decrease. As τ_c increases to 10 h, the mass flux gets broader and weakens. Figure 9 shows corresponding profiles of precipitation flux for the three different relaxation time scales. As τ_c decreases, the maximum precipitation increases and the width decreases in the same way as the mass flux distribution.

Figure 10 shows the variation of the width of the convecting region with relaxation time scale. We then consider the asymptotic limit of zero relaxation time. For relaxation time scales smaller than 6 h, the convective width is smaller than that of the SST, thus providing a simple explanation of the narrowing of convection reported by Back and Bretherton (2009). The convection region reduces to zero width in x. While somewhat artificial, the route toward this limit provides insight into how the efficiency of deep convection may influence the large scale. We will show later that very small values of τ_c are incompatible with our

boundary layer model, and thus physically unrealistic. The $\tau_c^{1/3}$ power law fits very well for small values of τ_c. This motivates a question: Does such a power law exist in weather and climate models? Fig. 11 shows the corresponding maximum mass flux, which, because of mass balance, varies as the reciprocal of the convective width. Halving the subsidence reduces the mass flux but doubling the SST anomaly increases it, following Eq. (12). The $\tau_c^{-1/3}$ power law also fits the maximum mass flux very well for small values of relaxation time scale.

b. Boundary layer moisture constraints

Figure 12 shows the variation of the nonconvective evaporation flux E_{nc} with relaxation time scale. The value of E_{nc} increases to 46 W m^{-2} from 24 W m^{-2} as the relaxation time scale decreases. Since E_{nc} is proportional to horizontal advection [Eq. (28)], it acts as an important boundary layer constraint. Figure 13 shows
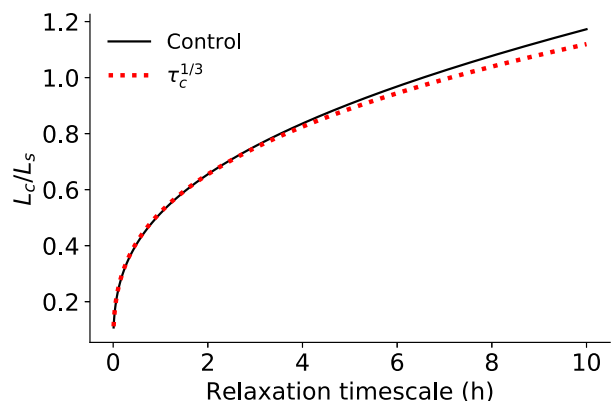

FIG. 10. The convective width (normalized by width of SST) plotted against convective relaxation time scale. Also shown is a $\tau_c^{1/3}$ power law (dotted).
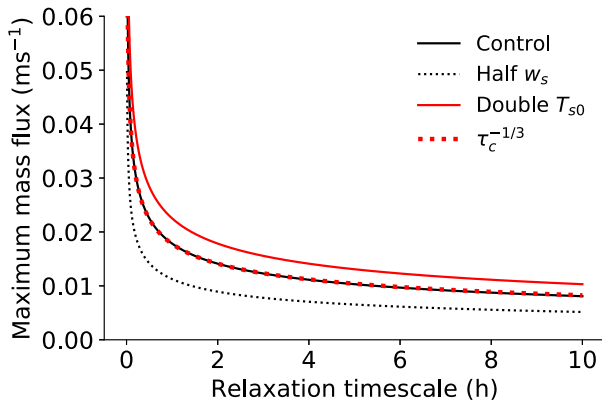
FIG. 11. Maximum mass flux plotted against convective relaxation time scale for the control (black), half subsidence (black dotted), and double SST anomaly (red) cases. Also shown is a $\tau_c^{-1/3}$ power law (red dotted).

FIG. 13. WTG moisture mixing ratio profile at the surface q_w (black) and the surface boundary layer maximum [max(q_s); red] plotted against τ_c.

that the maximum moisture mixing ratio also converges to the surface maximum as τ_c tends to zero.

Figure 14 shows horizontal winds for the boundary layer and upper troposphere. The sum of mass flux and subsidence decreases over the depth d below the tropopause, contributing to the divergence in the upper troposphere. The boundary layer convergence is proportional to the sum of the mass flux and the subsidence in the WTG layer. Since d is smaller than the boundary layer depth, the upper-tropospheric divergence is stronger than the boundary layer convergence.

c. Boundary layer balance maintaining CBL

Since the boundary layer–top vertical velocity matches the sum of subsidence and vertical velocity, its distribution is the same as shown in Fig. 8. Figure 15 shows the SST and the boundary layer potential
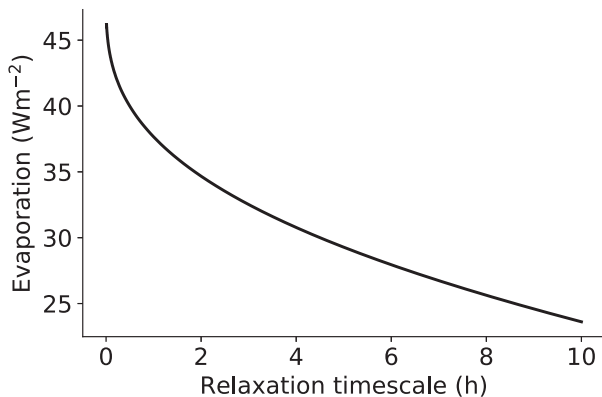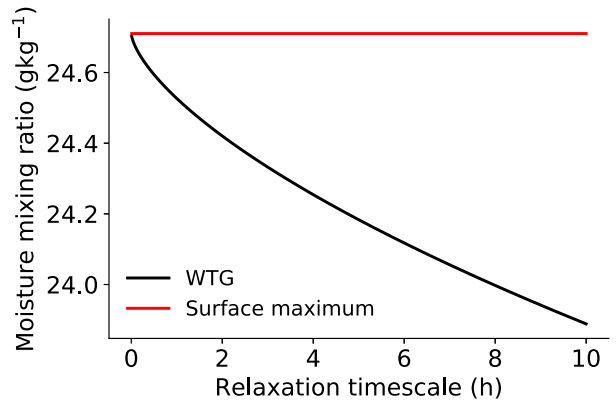
temperature for three different relaxation time scales. The boundary layer potential temperature curvature is proportional to the sum of the mass flux and the subsidence [Eq. (19)], so has negative curvature within the convection region, but positive curvature outside, intersecting the SST at the WTG value [Eq. (20)]. For $\tau_c = 2$ h, the values of the boundary layer potential temperature are less than the SST within the convection region. The boundary layer is thus clearly in the physically reasonable CBL state. When τ_c is decreased significantly to 0.4 h, the boundary layer potential temperature slightly exceeds the SST within the convective region, which is unrealistic. In contrast, when a value $\tau_c = 10$ h is used, the difference between the boundary layer and SST is smaller than 1 K at the sides of the domain, and boundary layer is clearly convective in the center.

Figure 16 shows the effect of significantly decreasing τ_b (increasing the drag). In this situation, the boundary

FIG. 12. The domain-averaged evaporation from the non-convecting region E_{nc}, plotted against convective relaxation time scale.
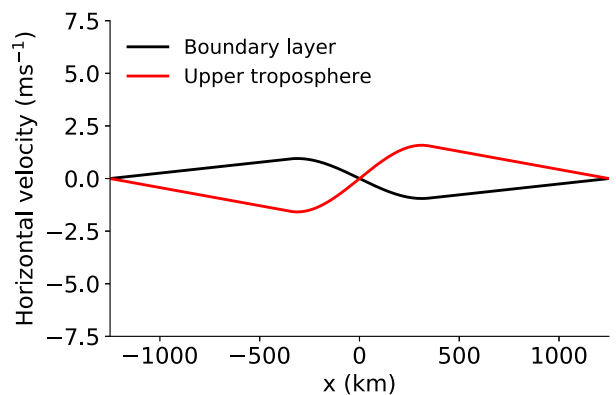

FIG. 14. Horizontal winds for boundary layer u_b (black) and upper troposphere u_u (red) for the control case.
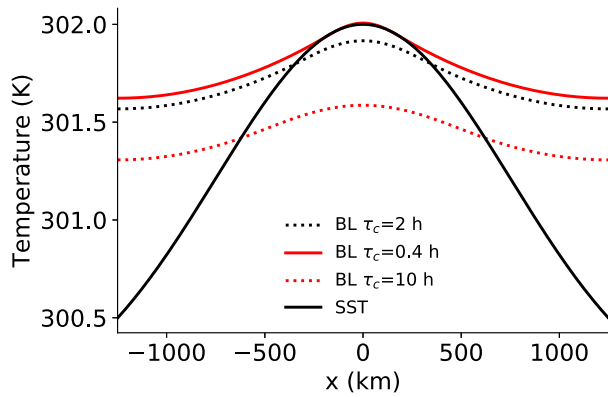
FIG. 15. The distribution of SST (black) and boundary layer potential temperature for $\tau_c = 2$ (black dotted), $\tau_c = 0.4$ (red), and $\tau_c = 10$ h (red dotted).

FIG. 17. The difference of the maximum SST from the maximum boundary layer potential temperature as a function of τ_b. Annotated are regions of CBL and SBL. The crossing point is at $\tau_b = 7.375$ h.

layer curvature has to increase significantly. The result is a boundary layer potential temperature that is greater than the SST. An SBL results in the convecting region, which is not realistic. Thus there is also a lower limit of τ_b (upper limit on drag) for maintaining a CBL beneath the convection. Figure 17 shows the difference between the maxima in SST and the boundary layer potential temperature; when this difference is positive, the boundary layer is in a CBL state (an SBL when negative). The crossover from CBL to SBL occurs at $\tau_b = 7.4$ h, and provides an upper limit on the boundary layer drag.

Figure 18 shows how the WTG temperature and the maximum boundary layer potential temperature both converge to the maximum SST as τ_c tends to zero. For the control, the maximum boundary layer temperature is less than the maximum SST (i.e., a CBL) for values of τ_c as small as 0.5 h; the boundary layer balance thus

sets a lower limit for τ_c. The minimum value is reduced significantly for the double τ_b case.

4. Discussion

In this paper, we have described a novel method for constructing a balanced boundary layer state that is consistent with WTG convection above. Such large-scale balanced states form helpful references against which to evaluate and understand full weather and climate models. The model combines, in a simple way, both the momentum and thermodynamic couplings identified by Sobel and Neelin (2006). The WTG state is taken as primary (Emanuel et al. 1994), and the boundary layer potential temperature distribution follows from it. This approach
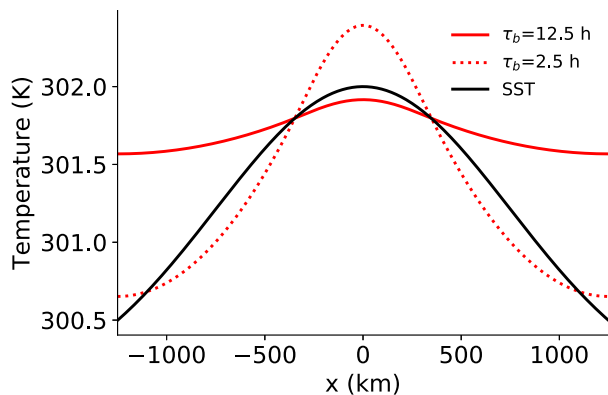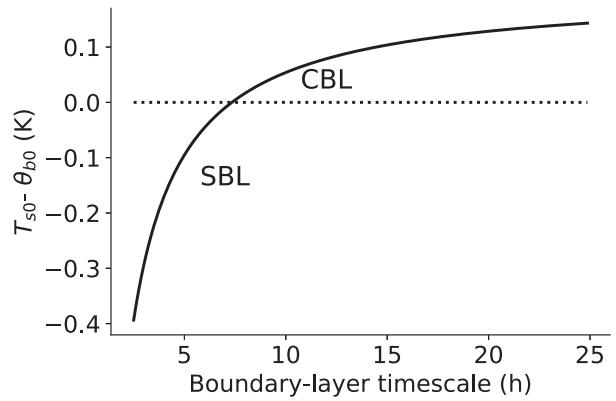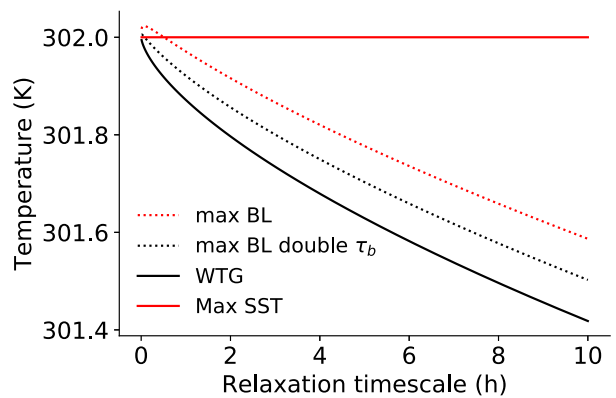

FIG. 16. The sensitivity of the boundary layer potential temperature to decreasing τ_b from 12.5 (red) to 2.5 h (red dotted), and increasing drag.

FIG. 18. WTG profile temperature at the surface (black) and maximum SST (red) plotted against τ_c. Also shown are the maximum boundary layer potential temperature for the control (red dotted) and double τ_b (black dotted) cases. The intersection of the maximum boundary layer potential temperature and the maximum SST (the change from CBL to SBL) is at $\tau_c = 0.5$ h for the control and $\tau_c = 0.1$ h for the double τ_b case.

contrasts with the view that the SST and boundary layer simply control the mass flux independent of the circulation above (Lindzen and Nigam 1987). The key findings from the model are

- The large-scale mass flux and width of convection are both functions of the relaxation time scale. The mass flux varies as $\tau_c^{-1/3}$, and width varies as its reciprocal. This relies on a uniform subsidence distribution with x and is also dependent on the shape of the SST distribution (Gaussian in this case).
- The large-scale mass flux and width also depend on the magnitude of the subsidence and the SST.
- The evaporation in the nonconvecting region constrains the horizontal moisture advection.
- Assuming Ekman balance, a positive horizontal curvature of the boundary layer potential temperature results. This relationship is consistent with the breakdown of the WTG in the tropical boundary layer.
- A convective boundary layer needs to be maintained beneath the mass flux. This means the drag has an upper limit (minimum τ_b). It also limits τ_c and L_c to minimum values. The minimum value of τ_b was 7.4 h, much larger than the minimum value of $\tau_c = 0.5$ h. This was due to the horizontal curvature of boundary layer potential temperature varying more rapidly with τ_b. The largest relaxation time scale used ($\tau_c = 10$ h) arguably gave the most realistic distribution of boundary layer potential temperature relative to the fixed SST. The commonly used value of $\tau_c = 2$ h (Betts 1986) probably reflects the omission of the north–south circulation, which will force convection quite strongly.

The issue of the horizontal distribution of mass flux is tackled here from a dynamical equilibrium and balanced boundary layer perspective. The role of gravity waves is implied by the maintenance of the WTG profile above the boundary layer, but not in the sense of horizontally distributing the subsidence in the way that happens over shorter time scales (Kuell et al. 2007). The width of the mass flux relies on a horizontally uniform subsidence. In this way, our model asks the question of weather and climate models: Is subsidence sufficiently horizontally distributed?

It is useful to place our model in context of similar ones in the literature. The model of Bretherton and Sobel (2002) is based on the moist static energy (MSE) budget and the strict quasi-equilibrium (SQE) assumption. It also relies on the definition of a gross moist stability in order to diagnose large-scale ascent. It does not include a frictional boundary layer. Our approach is thus an alternative to the SQE–MSE view that emphasizes the response to evaporation and radiation. While the width of

convection in Bretherton and Sobel (2002) is controlled by a simplified cloud feedback on the radiation, here the width is controlled by the convective time scale. We also note that there is still debate about the degree to which SQE applies to convection modeling (Raymond and Herman 2011). Our model also provides a basic-state circulation about which waves can develop. This is in contrast to the model of Wang and Rui (1990) that predicts the Kelvin wave response in the tropics.

There are other simplifications in our model that benefit from discussion. All the physics is linearized and often summarized by constants and time scales. The parameterizations of the boundary layer and convection were purposively minimal so that the dynamical effects were emphasized over the small-scale parameterization issues. Operational physical parameterization has some degree of nonlinearity. Nevertheless, the simple posing of physical constants provides a clearer perspective on coupling issues in more complicated weather and climate models. We have also restricted ourselves to east–west geometry. Additional effects such as the ascending branch of the Hadley circulation come into play when a north–south geometry is used.

Our model also exploits Ekman balance in the boundary layer. The balance assumption is applicable on time scales much greater than the boundary layer Rayleigh time scale (12.5 h); it is thus most applicable on time scales of weeks. We have also designed our convective parameterization with a common time scale τ_c for potential temperature and moisture mixing ratio. This provides both clarity and analytical convenience. We have assumed the constants of proportionality γ_c and γ_q. There is thus more scope to test these assumptions using observational data and climate models. For example, in a more comprehensive version of the model, one might consider varying the time scale with height (Raymond and Herman 2011).

In our model, causality currently proceeds as follows. The SST and relaxation time scale determine the magnitude and horizontal extent of the convective mass flux and the vertical temperature profile above the boundary layer. These determine the boundary layer flow and the evaporation in the nonconvecting region. If this evaporation exceeds that which is physically possible, it implies that the assumed relaxation time scale is unrealistic. Both boundary layer and convective processes contribute to the relaxation time scale as shown in Eq. (6). We do not attempt to estimate which contribution exerts the main control.

Parameterizations are often built from the small-scale process model and then inserted in the large-scale model. The hazard with this approach is that the interaction with the large scale is not fully evaluated during parameterization development. Here, we demonstrate

a different paradigm: starting from the large-scale balances (WTG, mass balance, and boundary layer balance) and understanding how the parameterizations work to preserve them. This helpfully changes the perspective and provides a new way of approaching model development.

Our model provides a useful framework for understanding dynamical feedbacks in more comprehensive models of the tropics and the role of the boundary layer in organizing larger-scale circulations. Here we have identified a power law in the convective efficiency for the narrowing of large-scale convection relative to the SST. We have also identified the role of the boundary layer in setting a lower limit on the convective width. Both these aspects could guide the design of new idealized tests of weather and climate models. For example, a series of test cases could be configured for a tropical domain with an SST anomaly, boundary layer convergence, and convection. As the boundary layer drag is increased, we could then test if an upper limit on

the drag is also required to maintain a CBL. We could also test if increasing the efficiency of the convection scheme (by varying appropriate parameters in a mass flux scheme) narrows the mass-flux distribution. Finally, further work could extend our model to north–south geometry, as previously noted.

APPENDIX

Fixed-Point Iteration

We now give the numerical iteration method for finding the convective width. We start by equating the maximum mass fluxes from the convection parameterization [Eq. (3)] and the mass balance [Eq. (8)], assuming the Gaussian SST distribution [Eq. (1)]:

$$M_{c0}\left[1 - \exp\left(-\frac{L_c^2}{4L_s^2}\right)\right]^{-1} = \frac{\gamma_c T_{s0}}{\tau_c} = -\frac{w_s L_x}{L_c}\left\langle \exp\left(-\frac{x^2}{L_s^2}\right) - \exp\left(-\frac{L_c^2}{4L_s^2}\right)\right\rangle^{-1}$$

$$= -\frac{w_s L_x}{L_c}\left[\frac{L_s}{L_c}\sqrt{\pi}\,\mathrm{erf}\left(\frac{L_c}{2L_s}\right) - \exp\left(-\frac{L_c^2}{4L_s^2}\right)\right]^{-1},$$

where erf is the error function. The solution is found by the fixed-point iteration

$$L_c = g(L_c), \tag{A1}$$

where g is a function. For a solution to exist, we require the absolute value of dg/dL_c to be less than one (Kharab and Guenther 2011). An appropriate choice of function was thus

$$g(L_c) = 2L_s\,\mathrm{erf}^{-1}\left[\frac{\mathscr{F}}{\sqrt{\pi}L_s} + \frac{L_c}{\sqrt{\pi}L_s}\exp\left(-\frac{L_c^2}{4L_s^2}\right)\right], \tag{A2}$$

where erf^{-1} is the inverse error function and

$$\mathscr{F} = -\frac{w_s L_x \tau_c}{\gamma_c T_{s0}}. \tag{A3}$$

REFERENCES

Back, L. E., and C. S. Bretherton, 2009: On the relationship between SST gradients, boundary layer winds, and convergence over the tropical oceans. *J. Climate*, **22**, 4182–4196, https://doi.org/10.1175/2009JCLI2392.1.

Beare, R. J., and M. J. P. Cullen, 2012: Balanced models of boundary-layer convergence. *Quart. J. Roy. Meteor. Soc.*, **138**, 1452–1464, https://doi.org/10.1002/qj.1877.

Betts, A. K., 1986: A new convective adjustment scheme. Part I: Observational and theoretical basis. *Quart. J. Roy. Meteor. Soc.*, **112**, 677–691, https://doi.org/10.1002/qj.49711247307.

Bretherton, C. S., and A. H. Sobel, 2002: A simple model of a convectively coupled Walker circulation using the weak temperature gradient approximation. *J. Climate*, **15**, 2907–2919, https://doi.org/10.1175/1520-0442(2002)015<2907:ASMOAC>2.0.CO;2.

Emanuel, K. A., J. D. Neelin, and C. S. Bretherton, 1994: On large-scale circulations in convecting atmospheres. *Quart. J. Roy. Meteor. Soc.*, **120**, 1111–1143, https://doi.org/10.1002/qj.49712051902.

Kharab, A., and R. G. Guenther, 2011: *An Introduction to Numerical Methods: A MATLAB Approach.* 3rd ed. Chapman and Hall/CRC Press, 576 pp.

Kuell, V., A. Gassmann, and A. Bott, 2007: Towards a new hybrid cumulus parametrization scheme for use in non-hydrostatic weather prediction models. *Quart. J. Roy. Meteor. Soc.*, **133**, 479–490, https://doi.org/10.1002/qj.28.

Lindzen, R. S., and S. Nigam, 1987: On the role of sea surface temperature gradients in forcing low-level winds and convergence in the tropics. *J. Atmos. Sci.*, **44**, 2418–2458, https://doi.org/10.1175/1520-0469(1987)044<2418:OTROSS>2.0.CO;2.

Naumann, A. K., B. Stevens, C. Hohenegger, and J. P. Mellado, 2017: A conceptual model of a shallow circulation induced by

prescribed low-level radiative cooling. *J. Atmos. Sci.*, **74**, 3129–3144, https://doi.org/10.1175/JAS-D-17-0030.1.

Press, W., S. Teukolsky, W. Vetterling, and B. Flannery, 2007: *Numerical Recipes: The Art of Scientific Computing.* 3rd ed. Cambridge University Press, 1256 pp.

Raymond, D. J., and X. Zeng, 2005: Modelling tropical atmospheric convection in the context of the weak temperature gradient approximation. *Quart. J. Roy. Meteor. Soc.*, **131**, 1301–1320, https://doi.org/10.1256/qj.03.97.

——, and M. J. Herman, 2011: Convective quasi-equilibrium reconsidered. *J. Adv. Model. Earth Syst.*, **3**, M08003, https://doi.org/10.1029/2011MS000079.

Seager, R., R. Murtugudde, A. Clement, and C. Herweijer, 2003: Why is there an evaporation minimum at the equator? *J. Climate*, **16**, 3793–3802, https://doi.org/10.1175/1520-0442(2003)016<3793:WITAEM>2.0.CO;2.

Sobel, A. H., and J. D. Neelin, 2006: The boundary layer contribution to intertropical convergence zones in the quasi-equilibrium tropical circulation model framework. *Theor. Comput. Fluid Dyn.*, **20**, 323–350, https://doi.org/10.1007/s00162-006-0033-y.

Stevens, B., J. Duan, J. C. McWilliams, M. Münnich, and J. D. Neelin, 2002: Entrainment, Rayleigh friction, and boundary layer winds over the tropical Pacific. *J. Climate*, **15**, 30–44, https://doi.org/10.1175/1520-0442(2002)015<0030:ERFABL>2.0.CO;2.

Wang, B., and H. Rui, 1990: Dynamics of the coupled moist Kelvin–Rossby wave on an equatorial β-plane. *J. Atmos. Sci.*, **47**, 397–413, https://doi.org/10.1175/1520-0469(1990)047<0397:DOTCMK>2.0.CO;2.